

Communication

Application of Rh/TiO₂ Nanotube Array in Photocatalytic Hydrogen Production from Formic Acid Solution

Mahmudul Hassan Suhag^{1,2}, Ikki Tateishi^{3,*}, Mai Furukawa¹, Hideyuki Katsumata¹, Aklima Khatun¹
and Satoshi Kaneco^{1,*}¹ Department of Chemistry for Materials, Graduate School of Engineering, Mie University, Tsu 514-8507, Mie, Japan² Department of Chemistry, University of Barishal, Barishal 8254, Bangladesh³ Mie Global Environment Center for Education & Research, Mie University, Tsu 514-8507, Mie, Japan* Correspondence: tateishi@gecer.mie-u.ac.jp (I.T.); kaneco@chem.mie-u.ac.jp (S.K.); Tel.: +81-59-231-9427 (S.K.)

Abstract: Titanium dioxide nanotubes (TNTs) were fabricated via electrochemical anodization process. Photocatalytic hydrogen generation from formic acid solution was investigated using TNTs with simultaneous Rh deposition. The effects of calcination temperature and time for TNTs on hydrogen generation were studied. The maximum hydrogen generation (54 μmol) was observed when using TNTs with a 500 °C calcination temperature and 10 h calcination time under 5 h of black light (352 nm) irradiation. The reusability tests indicated that the TNTs with photodeposited Rh metal (Rh/TNT) had excellent stability up to the fifth cycle for hydrogen generation from formic acid solution. The TNTs were characterized before and after photodeposition of Rh metal via X-ray powder diffraction (XRD), scanning electron microscopy (SEM), photoluminescence (PL), and diffuse reflectance spectroscopy (DRS). XRD revealed the presence of optimal anatase–rutile phase ratios in TNTs at 500 °C and 300 °C calcination temperatures. XRD and SEM revealed the deposition of Rh metal on the TNT surface at 300 °C and 500 °C calcination temperatures. It was observed that the light absorption ability of TNTs calcined at 500 °C was greater than that of TNTs calcined at 300 °C. The reaction mechanisms for the formation of TNTs and photocatalytic hydrogen production from formic acid solutions by TNTs with simultaneous Rh deposition were also proposed.

Keywords: nanotube TiO₂; H₂ production; deposition of Rh; formic acid; calcination



Citation: Suhag, M.H.; Tateishi, I.; Furukawa, M.; Katsumata, H.; Khatun, A.; Kaneco, S. Application of Rh/TiO₂ Nanotube Array in Photocatalytic Hydrogen Production from Formic Acid Solution. *J. Compos. Sci.* **2022**, *6*, 327. <https://doi.org/10.3390/jcs6110327>

Academic Editor: Vincenza Brancato

Received: 15 September 2022

Accepted: 31 October 2022

Published: 2 November 2022

Publisher's Note: MDPI stays neutral with regard to jurisdictional claims in published maps and institutional affiliations.



Copyright: © 2022 by the authors. Licensee MDPI, Basel, Switzerland. This article is an open access article distributed under the terms and conditions of the Creative Commons Attribution (CC BY) license (<https://creativecommons.org/licenses/by/4.0/>).

1. Introduction

Today, the energy crisis issue is one of the most important topics around the world. Hydrogen may be considered a significant energy source for the future, because it has clean, sustainable, environmentally benign, and renewable properties [1–4]. Compared to conventional hydrogen production techniques, photocatalytic hydrogen production from water may be an environmentally friendly and cost-effective method, owing to the abundance of solar light and the availability of photocatalysts. In this method, the photocatalyst utilizes the energy of absorbed light from the sun to reduce the protons of water to hydrogen energy [2,5,6].

The photocatalyst TiO₂ is one of most widely used catalysts for hydrogen generation from water, because of its nontoxicity, commercial availability, chemical stability, and photostability [7–10]. Since TiO₂ has a relatively large band gap with relatively rapid recombination of electron hole pair, only UV light can be utilized for hydrogen production [7–9]. Hence, different approaches have been adopted in order to improve the photocatalytic hydrogen generation efficiency of TiO₂, such as doping with metal and nonmetal ions, coupling with other semiconductors, supporting metallic or nonmetallic oxides, using organic sacrificial agents, and varying the size of nanoparticles [8,11–13].

For instance, many research articles have been published on doping of TiO₂ with Pt, Au, Ag, Rh, and Pd noble metals for the improvement of the photocatalytic hydrogen

generation reaction [14–17]. Various methods such as the chemical reduction method, sono-chemical reduction method, dispersion method, photochemical deposition method, deposition–precipitation method, and sol–gel method have been reported for doping metal onto TiO₂ nanoparticles [18]. In the photochemical deposition method, a metal ion can be reduced to a metal atom by accepting the photogenerated electron in the conduction band of TiO₂ and can be deposited onto the surface of TiO₂. Then, another photogenerated electron can transfer to the deposited metal atom, and the movement of electrons can decrease the electron hole pair recombination rate [18,19].

Organic sacrificial agents such as formic acid, ethanol, and glycerol act as hole scavengers in the valance band of TiO₂ by donating electrons [12]. Therefore, organic sacrificial methods have been widely applied in photochemical hydrogen generation.

Titanium dioxide nanotubes (TNTs) are highly attractive for photocatalytic applications due to their large surface area, high physical stability, good adsorption ability, superior electron transport rate, and excellent photoelectrochemical properties. Furthermore, TNTs can be used more repeatedly and conveniently than TiO₂ powder [5,20–24]. Hence, the fabrication of TNTs for photochemical generation of hydrogen has recently attracted extensive research. There are several preparative methods for TNT formation, such as hydrothermal, sol–gel, template-assisted, and electrochemical anodization methods [25–29]. The electrochemical anodization method has several advantages compared to other methods. The anodization method is simple, and the geometry of the nanotubes can be controlled by regulating experimental constraints such as oxidation electrode potential, concentration of the electrolyte, anodization time, and calcination temperature. TNT arrays with a desired length and thickness can be synthesized using this method [1,30].

Rh-doped TiO₂ photocatalysts have high photocatalytic properties [31]. Previously, we reported on photocatalytic hydrogen production from a formic acid solution with TiO₂ with the aid of simultaneous Rh deposition [32]. It was observed that under optimal conditions, the photocatalytic hydrogen generation rate with the aid of simultaneous photodeposition of Rh metal onto TiO₂ was about 250 times better than that obtained with bare TiO₂.

In the present study, TNTs were fabricated via the electrochemical anodization method, and photocatalytic hydrogen production from formic acid solution using TNTs was investigated with the simultaneous photodeposition of Rh metal. The effects of calcination temperature and time for TNTs on the photocatalytic hydrogen production efficiency from formic acid solution were evaluated. The reusability of Rh/TNTs for the production of hydrogen from formic acid was also monitored. The TNTs were characterized before and after photodeposition of Rh metal using X-ray diffraction (XRD), scanning electron microscopy (SEM), photoluminescence spectra, and diffuse reflectance spectra.

2. Materials and Methods

2.1. Fabrication of TiO₂ Nanotubes (TNTs)

The TNTs were fabricated via anodization of a titanium plate (1.0 × 7.0 cm), according to a previous research report with minor modifications [33]. In brief, a titanium plate was connected to the anode and a platinum plate was connected to the cathode of an electrolytic cell. Hydrofluoric acid aqueous solution (1 wt%) was used as the electrolyte. To prepare the TNTs, the Ti plate was anodized under ultrasonic treatment with a DC constant voltage/current power of 20 V for 30 min. After anodization of the Ti plate, the fabricated electrode was washed with methanol and deionized water. Finally, it was calcined at high temperatures (300–700 °C) for 1–20 h under an air atmosphere using an electric furnace in order to improve the crystallinity of the TNTs.

2.2. Photocatalytic Hydrogen Production

Hydrogen production with TNTs was performed with simultaneous Rh deposition [19]. The concentration of formic acid, amount of Rh³⁺, solution pH, and temperature were chosen based on the optimal conditions identified in our previous work [32]. A Pyrex column vessel reactor (inner volume 35 mL) was used for the photocatalytic hydrogen

production from formic acid. Formic acid solution (25 mL) was added to the reactor. Then, a TNT plate (1.0 × 5.0 cm) was added to the reactor. Next, RhCl₃ solution (Rh concentration: 2 mg L⁻¹) was added to the reactor. A 15 W black lamp with about 352 nm emission (Toshiba Lighting & Technology Corp., Tokyo, Japan) was placed to the side of the Pyrex vessel reactor as a light source. The light intensity was measured using a UV radio meter (UIT-201, Ushio Inc., Tokyo, Japan), and the value was 0.25 mW/cm². The formic acid solution was continuously stirred in the presence of TNTs by a magnetic stirrer during the light irradiation. Using a hot stirrer, the reactor temperature was kept constant at 50 °C. The reactor was sealed with a silicon septum. The irradiation time was 1~5 h. The produced H₂ was extracted from the upper part of the reactor with a microsyringe (ITO, Co., Ltd., Tokyo, Japan) and measured using a gas chromatograph (GL Sciences, GC-3200, Tokyo, Japan) with a thermal conductivity detector. A stainless column (4 m long, 2.17 mm i.d.) packed with Molecular Sieve 5A (mesh 60–80) was used for the separation. The carrier gas was 99.9% argon gas (Kawase Sangyo Co., Ltd., Kuwana, Mie, Japan). The temperature conditions of GC were 50 °C for the injection, column, and detector. The flow rate of the carrier gas was 7.0 mL/min.

Analysis time and analysis sample amount were 10 min and 250 µL, respectively. The reproducibility of H₂ generation was investigated, and relative standard deviations (RSDs) were observed within 10% for more than three runs.

2.3. Characterization of TNTs

Before and after the light irradiation, the characteristics of TNTs fabricated under different calcination conditions were evaluated by SEM image, X-ray diffraction (XRD), photoluminescence spectrum (PL), and diffuse reflection spectrum (DRS) measurements. XRD measurements were performed using a Rigaku RINT Ultima-IV diffractometer with Cu radiation at a scan rate of 0.04°/s in a scan range of 10–80°. In order to monitor the morphology of the TiO₂ nanotubes, SEM observations were performed using a Hitachi S-4000 SEM with an accelerating voltage of 25 kV. PL spectra of TNTs were observed using a RF-5300PC spectrofluorophotometer (SHIMADZU, Kyoto, Japan). The diffuse reflectance spectra of the TNTs were measured with a UV2450 UV–vis system (SHIMADZU, Kyoto, Japan). BaSO₄ was used as a reference material in the diffuse reflectance spectral measurements.

3. Results and Discussion

3.1. Characterization of TNTs

SEM images of TNTs fabricated at different calcination temperatures before and after light irradiation (TNTs and Rh/TNTs, respectively) are shown in Figure 1. A similar shape (tube with a 60 nm average diameter) was confirmed before and after light irradiation for TNTs prepared at 300 °C and 500 °C calcination temperatures. The phase crystallinities for TNTs fabricated at less than 500 °C could be related to anatase TiO₂. The length of the nanotube arrays was approximately 400 nm. On the other hand, the shape and structure of the nanotubes prepared at a 700 °C calcination temperature were degraded. These results indicated that the tubular morphology of TNTs was stable at calcination temperatures of up to 500 °C. Although large Rh particles with a diameter of 400–600 nm were deposited on the TNT surface after the irradiation with light at 300 and 500 °C calcination temperatures, small particles for Rh may be modified onto the inner surface of the TNTs.

The XRD spectra of TNTs prepared at different calcination temperatures were analyzed before and after light irradiation. The results are illustrated in Figure 2, and the standard card JCPDS is shown in Figure S1 (Supporting Information) as the reference. A strong rutile phase peak was observed at $2\theta = 27.5^\circ$ for TNTs calcined at 700 °C before and after light irradiation. The peak observed at $2\theta = 27.5^\circ$ corresponded to the (110) plane for a rutile crystalline structure [34]. This peak was not observed for TNTs prepared at 300 °C and 500 °C calcination temperatures, which indicated different rutile and anatase phase ratios. Moreover, similar peak positions were observed in the XRD patterns for TNTs prepared at 300 °C and 500 °C calcination temperatures before and after light irradiation. Since there

was no Rh peak in the XRD pattern, it seems that the Rh metal was well deposited on the TNT surface.

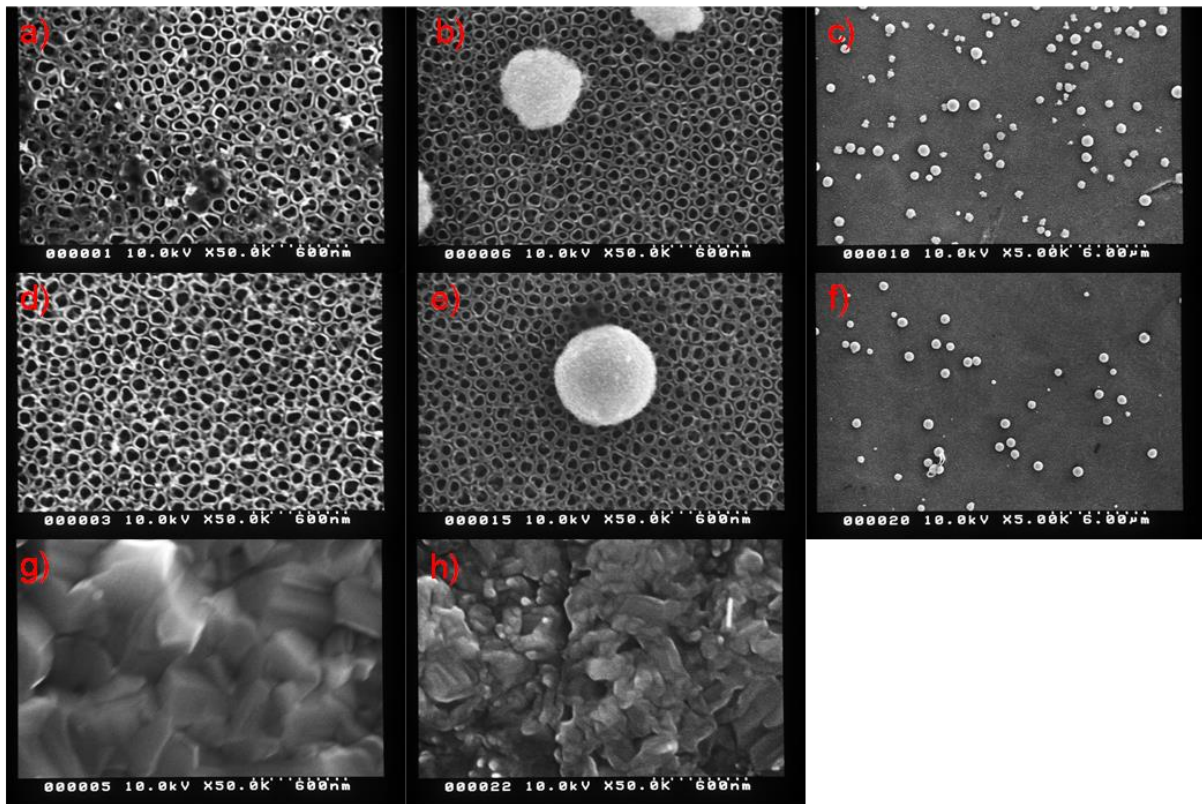


Figure 1. SEM images of TNTs. Calcination temperature: 300 °C for (a–c), 500 °C for (d–f), and 700 °C for (g,h). (a,d,g) before irradiation. (b,c,e,f,h) after irradiation.

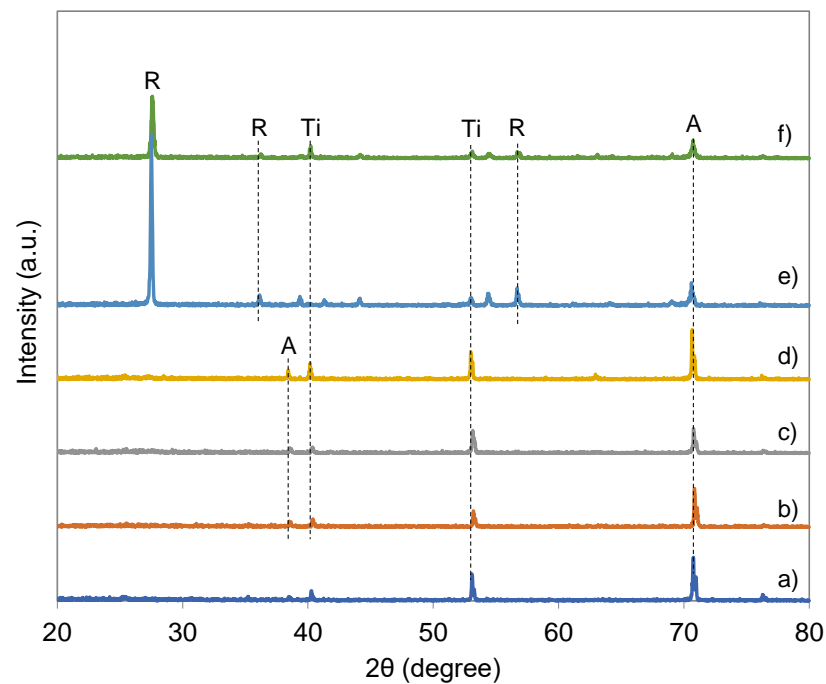


Figure 2. XRD patterns of TNTs. Calcination temperature: 300 °C for (a,b), 500 °C for (c,d), and 700 °C for (e,f). (a,c,e) before irradiation. (b,d,f) after irradiation.

Generally, the suppression of photogenerated electron hole pair recombination is responsible for weak fluorescence intensity, because more recombinations of excited electron hole pairs give more PL emission intensity [35]. As shown in Figure 3, the peak intensities of the PL spectra for TNTs prepared at 300 °C calcination temperatures were lower than those obtained at 500 °C calcination temperatures, although their shapes were almost the same.

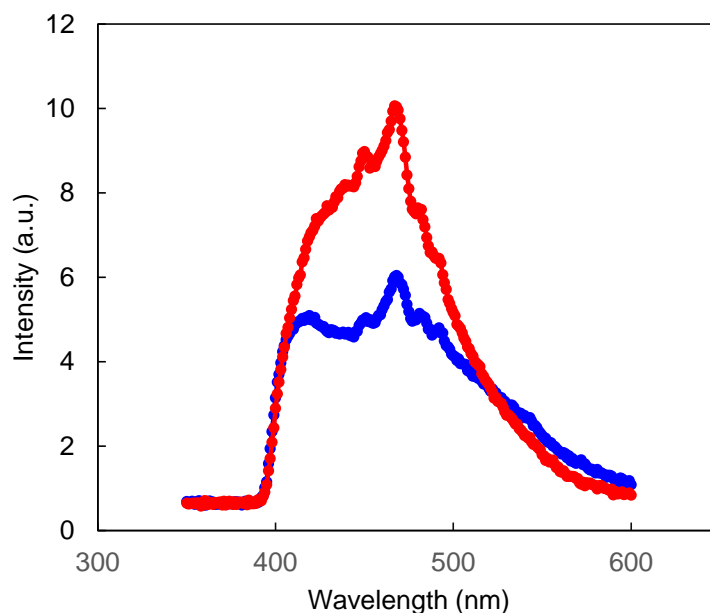


Figure 3. Photoluminescence spectra for TNTs. Calcination temperature: blue line for 300 °C and red line for 500 °C. Since the TNTs were subjected to PL analysis after irradiation, the Rh metal was modified onto the surface of TNTs.

UV–vis diffuse reflection spectroscopy (DRS) was used to evaluate the absorption edges and band gaps of TNTs fabricated at different calcination temperatures. Hence, the TNTs were evaluated using DRS after the photodeposition of Rh metal. Since the absorption wavelength in a semiconductor is generally correlated to the band gap, the band gap decreases with red-shifting absorption edges [36]. UV–vis reflectance spectra were converted to absorbance according to the Kubelka–Munk equation (Figure 4a). Using Tauc plots (plotting $\alpha h\nu$ vs $h\nu$), as shown in Figure 4b, the band gap energy of photocatalysts can be determined [37]. As shown in the figure, significant absorptions were scarcely observed for TNTs fabricated at 700 °C. Though the band gap for Rh/TNTs prepared at 500 °C calcination temperature was slightly larger than that of those prepared at 300 °C, a greater absorption ability below 380 nm was observed for those prepared at 500 °C, relative to those prepared at 300 °C.

3.2. Effect of Calcination Temperature

It was reported in a previous paper [32] that the optimum conditions for photocatalytic hydrogen production were 1.0 wt% formic acid concentration, solution pH 2.2, and reaction temperature 50 °C. Therefore, the subsequent experiments with photocatalytic H₂ production were performed under these experimental conditions.

The effect of calcination temperature use for the synthesis of TNTs on the photocatalytic production of hydrogen using TNTs with simultaneous deposition of Rh metal was investigated. The results are shown in Figure 5. It can be seen that the amount of hydrogen production was the highest with the TNTs calcined at 500 °C. Generally, a reduction of recombination frequency of electrons and holes causes the enhancement of photocatalytic activity. The recombination of electrons and holes seems to be decreased by the coexistence of anatase and rutile phases for efficient charge separation at the phase junction [38].

Here, the optimal anatase and rutile phase ratio and their crystallinities may have been responsible for the maximum photocatalytic activity associated with TNTs prepared at a 500 °C calcination temperature. The results may be due to the fact that the light absorption ability of Rh/TNTs prepared at 500 °C calcination temperatures was better relative to that observed at 300 °C calcination temperatures. At a 700 °C calcination temperature, the existence of more anatase phase and the collapse of tubular morphology of TNTs could be the cause of the poor photocatalytic activity.

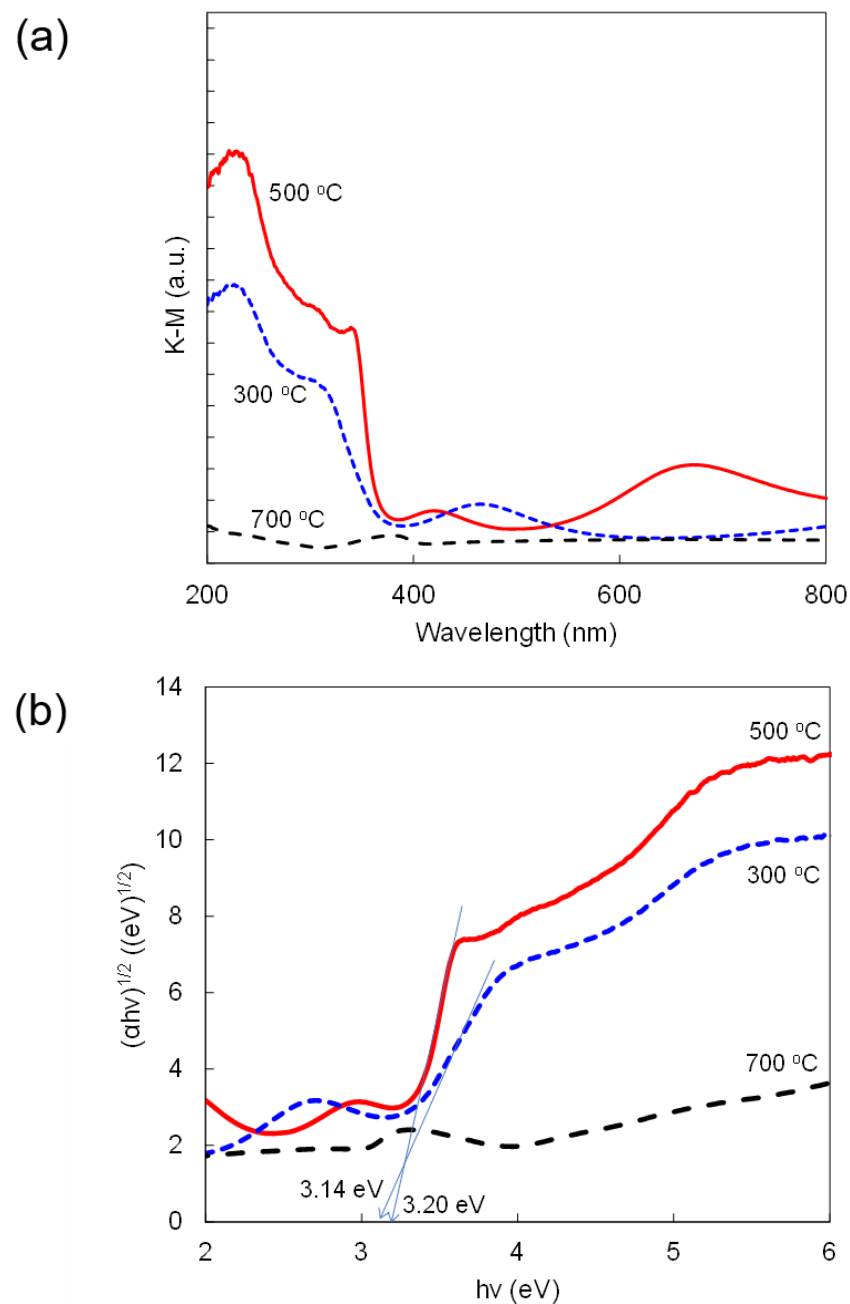


Figure 4. UV-vis Kubelka–Munk transformed diffuse reflectance spectra (a) and Tauc plot (b). Since the TNTs were subjected to UV-vis analysis after irradiation, the Rh metal was modified onto the surface of TNTs. Calcination temperature: blue line for 300 °C, red line for 500 °C, and black line for 700 °C.

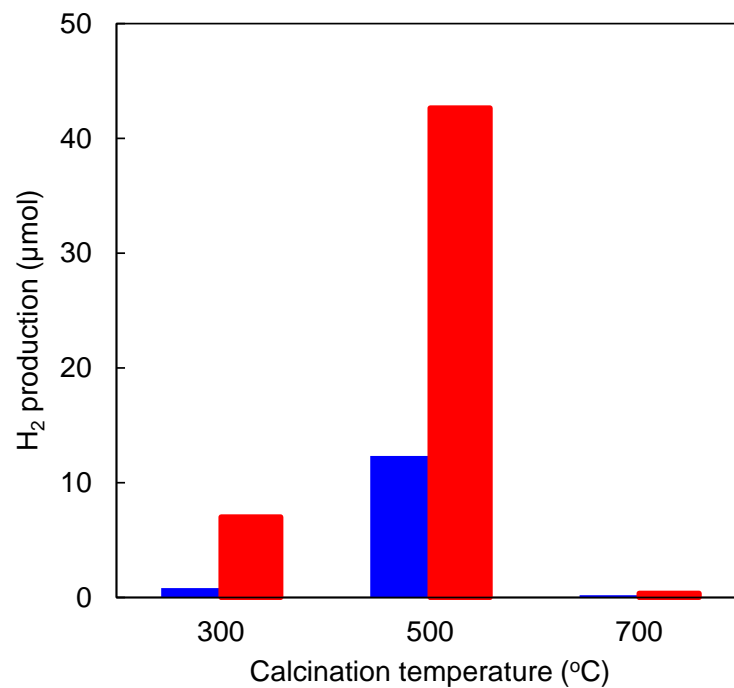


Figure 5. Effect of calcination temperature on photocatalytic H₂ production from formic acid with TiO₂ nanotubes with the aid of simultaneous Rh deposition. Reaction time: 3 h (blue bar) and 5 h (red bar); reaction temperature: 50 °C; calcination time: 2 h.

3.3. Effect of Calcination Time

The effect of calcination time in the fabrication of TNTs on the photocatalytic hydrogen production with TNTs was monitored. The results are illustrated in Figure 6. It was observed that the hydrogen production was highest (54 μmol) after 5 h of black light irradiation with TNTs fabricated via 10 h calcination at 500 °C. Better crystallinity of TNTs would be formed at 10 h of calcination at 500 °C, improving the electron hole pair formation rate. Hence, the optimum calcination conditions of 500 °C for 10 h were selected for photocatalytic hydrogen production from formic acid solutions.

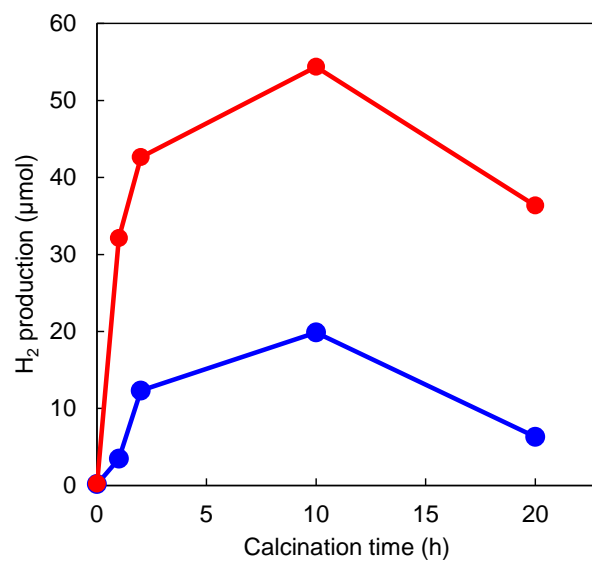


Figure 6. Effect of calcination time on photocatalytic H₂ production from formic acid with TiO₂ nanotubes with the aid of simultaneous Rh deposition. Reaction time: 3 h (blue line) and 5 h (red line); reaction temperature: 50 °C; calcination temperature: 500 °C.

3.4. Reusability of TNT Photocatalysts

In order to check the stability and reusability of the Rh/TNT photocatalysts, the hydrogen production from a formic acid solution was observed for five cycles. The TNTs prepared under the optimum conditions (500 °C for 10 h) were used. The results are shown in Figure 7. The data showed that the photocatalytic activity for hydrogen production was a little lower after the five runs, and there was no obvious loss of the photocatalytic hydrogen production activity in the subsequent run. It was indicated that the high chemical stability of Rh/TNTs for hydrogen production from formic acid solution could be confirmed by catalyst lifetime tests.

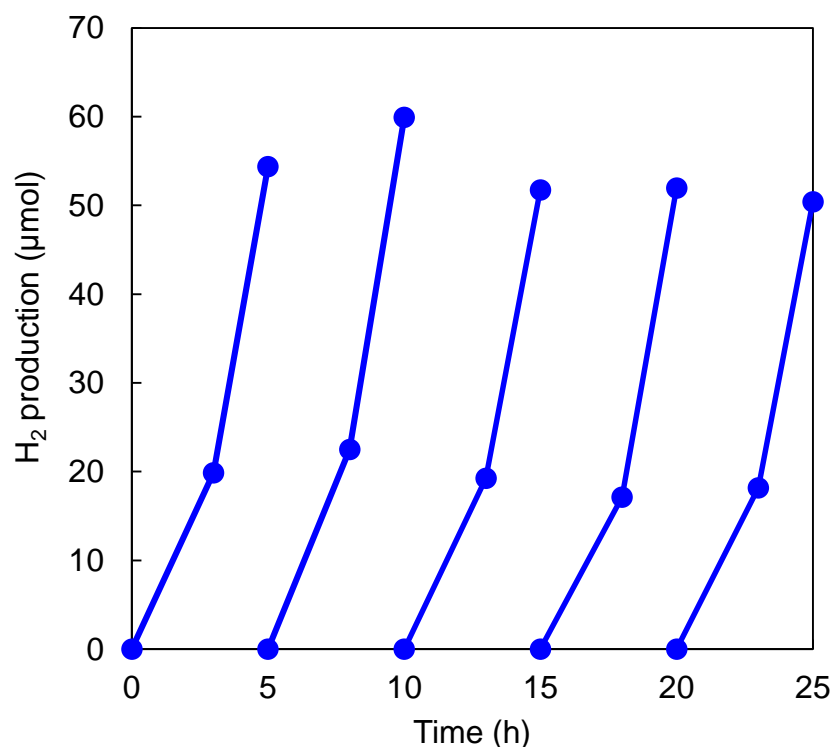
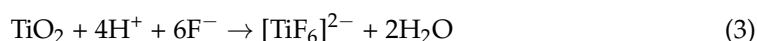


Figure 7. Cycled performance of photocatalytic H₂ production from formic acid with TiO₂ nanotubes with the aid of simultaneous Rh deposition. Reaction temperature: 50 °C; calcination temperature: 500 °C; calcination time: 10 h.

3.5. Mechanism of Hydrogen Production

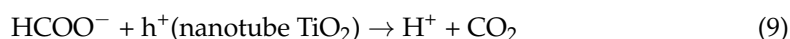
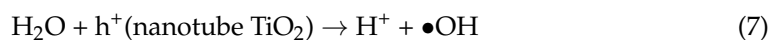
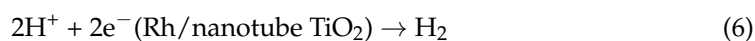
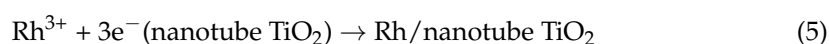
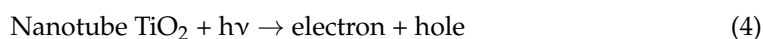
On the basis of the present study and previous literature for the formation of TNTs, the possible mechanism of fabrication of TNTs is proposed as follows [39–41]. The reaction occurring in the formation of TNTs by anodization of titanium plate is given as follows:



(a) A layer of TiO₂ is formed on the titanium plate. (b) The layer of TiO₂ is cracked, and pores are formed due to the formation of crystals. (c) A complex is formed by the reaction of fluorine ions with TiO₂, and the pores grow due to the dissolution of TiO₂. (d) Simultaneously, the TiO₂ layer also undergoes repassivation. (e) After that, a void is formed between the pores. (f) As a result, TNTs are formed on the surface of the Ti sheet.

The mechanism for photocatalytic H₂ production from formic acid solution using TNTs with the aid of simultaneous Rh deposition is shown in Equations (4) to (9). An electron and hole pair is formed after irradiation with light with a wavelength less than

the band gap on the TNTs. In addition, Rh^{3+} is reduced to Rh metal, and the Rh metal is deposited on the surface of TNTs. Then, the photogenerated electrons move from the TNTs to Rh metal, and the movement of electrons can suppress the recombination of electrons and holes. It is considered that the formate ions oxidize with photogenerated holes to generate protons and CO_2 . The generated protons can be reduced on the surface of the Rh metal to generate hydrogen gas. The optimum calcination temperature for TNTs for the photocatalytic H_2 production from formic acid with the aid of simultaneous Rh deposition was $500\text{ }^\circ\text{C}$. Because the intensity of PL for TNTs prepared with a calcination temperature of $500\text{ }^\circ\text{C}$ was greater compared with that of TNTs prepared at a calcination temperature of $300\text{ }^\circ\text{C}$, the optimum calcination temperature could be attributed to better light absorption ability and the crystallinities of Rh/TNTs prepared at $500\text{ }^\circ\text{C}$.



4. Conclusions

TNTs were synthesized via electrochemical anodization method, and the TNTs showed excellent photocatalytic activity in hydrogen generation from formic acid solution with the simultaneous deposition of Rh metal. The Rh-doped TNTs had admirable reusability and were very stable up to the fifth cycle. The optimum calcination conditions were $500\text{ }^\circ\text{C}$ over 10 h for photocatalytic H_2 production from formic acid solution with the aid of simultaneous Rh deposition.

Supplementary Materials: The following supporting information can be downloaded at: <https://www.mdpi.com/article/10.3390/jcs6110327/s1>, Figure S1: Tetragonal anatase phase (JCPDs file no. 21-1272, space group I41 /amd) and the tetragonal rutile phase (JCPDs file no. 21-1276, space group P42 /mnm) for TiO_2 .

Author Contributions: Conceptualization, M.H.S.; investigation, M.F.; data curation, M.F.; writing—original draft preparation, M.H.S. and I.T.; writing—review and editing, H.K. and A.K.; supervision, S.K. All authors have read and agreed to the published version of the manuscript.

Funding: This research was partially funded by Grant-in-Aid for Scientific Research (B) 21H03642 from the Ministry of Education, Culture, Sports, Science, and Technology of Japan.

Institutional Review Board Statement: Not applicable.

Informed Consent Statement: Not applicable.

Data Availability Statement: Not applicable.

Acknowledgments: The authors acknowledge Kengo Minamibata for the experimental supports.

Conflicts of Interest: All experiments were conducted at Mie University. Any opinions, findings, conclusions or recommendations expressed in this paper are those of the authors and do not necessarily reflect the view of the supporting organizations.

References

1. Ge, M.; Li, Q.; Cao, C.; Huang, J.; Li, S.; Zhang, S.; Chen, Z.; Zhang, K.; Al-Deyab, S.S.; Lai, Y. One-dimensional TiO_2 nanotube photocatalysts for solar water splitting. *Adv. Sci.* **2017**, *4*, 1600152. [[CrossRef](#)] [[PubMed](#)]
2. Tahir, M.; Tasleem, S.; Tahir, B. Recent development in band engineering of binary semiconductor materials for solar driven photocatalytic hydrogen production. *Int. J. Hydrogen Energy* **2020**, *45*, 15985–16038. [[CrossRef](#)]

3. Trang, T.N.Q.; Nam, N.D.; Tu, L.T.N.; Quoc, H.P.; Van Man, T.; Ho, V.T.T.; Thu, V.T.H. In situ spatial charge separation of an Ir@TiO₂ multiphase photosystem toward highly efficient photocatalytic performance of hydrogen production. *J. Phys. Chem. C* **2020**, *124*, 16961–16974. [[CrossRef](#)]
4. Wang, X.; Zhang, S.; Peng, B.; Wang, H.; Yu, H.; Peng, F. Enhancing the photocatalytic efficiency of TiO₂ nanotube arrays for H₂ production by using non-noble metal cobalt as co-catalyst. *Mater. Lett.* **2016**, *165*, 37–40. [[CrossRef](#)]
5. Denisov, N.; Yoo, J.E.; Schmuki, P. Effect of different hole scavengers on the photoelectrochemical properties and photocatalytic hydrogen evolution performance of pristine and Pt-decorated TiO₂ nanotubes. *Electrochim. Acta* **2019**, *319*, 61–71. [[CrossRef](#)]
6. Do, H.H.; Nguyen, D.L.T.; Nguyen, X.C.; Le, T.H.; Nguyen, T.P.; Trinh, Q.T.; Ahn, S.H.; Vo, D.V.N.; Kim, S.Y.; Le, Q.V. Recent progress in TiO₂-based photocatalysts for hydrogen evolution reaction: A review. *Arab. J. Chem.* **2020**, *13*, 3653–3671. [[CrossRef](#)]
7. Corredor, J.; Rivero, M.J.; Rangel, C.M.; Gloaguen, F.; Ortiz, I. Comprehensive review and future perspectives on the photocatalytic hydrogen production. *J. Chem. Technol. Biotechnol.* **2019**, *94*, 3049–3063. [[CrossRef](#)]
8. Feil, A.F.; Migowski, P.; Scheffer, F.R.; Pierozan, M.D.; Corsetti, R.R.; Rodrigues, M.; Pezzi, R.P.; Machado, G.; Amaral, L.; Teixeira, S.R.; et al. Growth of TiO₂ nanotube arrays with simultaneous Au nanoparticles impregnation: Photocatalysts for hydrogen production. *J. Braz. Chem. Soc.* **2010**, *21*, 1359–1365. [[CrossRef](#)]
9. Fiorenza, R.; Sciré, S.; D'Urso, L.; Compagnini, G.; Bellardita, M.; Palmisano, L. Efficient H₂ production by photocatalytic water splitting under UV or solar light over variously modified TiO₂-based catalysts. *Int. J. Hydrogen Energy* **2019**, *44*, 14796–14807. [[CrossRef](#)]
10. Ou, W.; Pan, J.; Liu, Y.; Li, S.; Li, H.; Zhao, W.; Wang, J.; Song, C.; Zheng, Y.; Li, C. Two-dimensional ultrathin MoS₂-modified black Ti³⁺-TiO₂ nanotubes for enhanced photocatalytic water splitting hydrogen production. *J. Energy Chem.* **2020**, *43*, 188–194. [[CrossRef](#)]
11. Anpo, M.; Shima, T.; Kodama, S.; Kubokawa, Y. Photocatalytic hydrogenation of CH₃CCH with H₂O on small-particle TiO₂: Size quantization effects and reaction intermediates. *J. Phys. Chem.* **1987**, *91*, 4305–4310. [[CrossRef](#)]
12. Clarizia, L.; Spasiano, D.; Di Somma, I.; Marotta, R.; Andreozzi, R.; Dionysiou, D.D. Copper modified-TiO₂ catalysts for hydrogen generation through photoreforming of organics. A short review. *Int. J. Hydrogen Energy* **2014**, *39*, 16812–16831. [[CrossRef](#)]
13. Thompson, T.L.; Yates, J.T. Surface science studies of the photoactivation of TiO₂—New photochemical processes. *Chem. Rev.* **2006**, *106*, 4428–4453. [[CrossRef](#)] [[PubMed](#)]
14. Gomathisankar, P.; Kawamura, T.; Katsumata, H.; Suzuki, T.; Kaneco, S. Photocatalytic hydrogen production from aqueous methanol solution using titanium dioxide with the aid of simultaneous metal deposition. *Energy Sources Part A Recover. Util. Environ. Eff.* **2016**, *38*, 110–116. [[CrossRef](#)]
15. Kumaravel, V.; Mathew, S.; Bartlett, J.; Pillai, S.C. Photocatalytic hydrogen production using metal doped TiO₂: A review of recent advances. *Appl. Catal. B Environ.* **2019**, *244*, 1021–1064. [[CrossRef](#)]
16. Liu, S.X.; Qu, Z.P.; Han, X.W.; Sun, C.L. A mechanism for enhanced photocatalytic activity of silver-loaded titanium dioxide. *Catal. Today* **2004**, *95–95*, 877–884. [[CrossRef](#)]
17. Sakthivel, S.; Shankar, M.V.; Palanichamy, M.; Arabindoo, B.; Bahnemann, D.W.; Murugesan, V. Enhancement of photocatalytic activity by metal deposition: Characterization and photonic efficiency of Pt, Au and Pd deposited on TiO₂ catalyst. *Water Res.* **2004**, *38*, 3001–3008. [[CrossRef](#)]
18. Gupta, B.; Melvin, A.A.; Matthews, T.; Dash, S.; Tyagi, A.K. TiO₂ modification by gold (Au) for photocatalytic hydrogen (H₂) production. *Renew. Sustain. Energy Rev.* **2016**, *58*, 1366–1375. [[CrossRef](#)]
19. Gomathisankar, P.; Yamamoto, D.; Katsumata, H.; Suzuki, T.; Kaneco, S. Photocatalytic hydrogen production with aid of simultaneous metal deposition using titanium dioxide from aqueous glucose solution. *Int. J. Hydrogen Energy* **2013**, *38*, 5517–5524. [[CrossRef](#)]
20. Divyasri, Y.V.; Reddy, N.L.; Lee, K.; Sakar, M.; Rao, V.N.; Venkatramu, V.; Shankar, M.V.; Reddy, N.C.G. Optimization of N doping in TiO₂ nanotubes for the enhanced solar light mediated photocatalytic H₂ production and dye degradation. *Environ. Pollut.* **2021**, *269*, 116170. [[CrossRef](#)]
21. Gong, J.; Pu, W.; Yang, C.; Zhang, J. Novel one-step preparation of tungsten loaded TiO₂ nanotube arrays with enhanced photoelectrocatalytic activity for pollutant degradation and hydrogen production. *Catal. Commun.* **2013**, *36*, 89–93. [[CrossRef](#)]
22. Huang, Q.; Gao, T.; Niu, F.; Chen, D.; Chen, Z.; Qin, L.; Sun, X.; Huang, Y.; Shu, K. Preparation and enhanced visible-light driven photocatalytic properties of Au-loaded TiO₂ nanotube arrays. *Superlattices Microstruct.* **2014**, *75*, 890–900. [[CrossRef](#)]
23. Zhang, S.; Wang, H.; Yeung, M.; Fang, Y.; Yu, H.; Peng, F. Cu(OH)₂-modified TiO₂ nanotube arrays for efficient photocatalytic hydrogen production. *Int. J. Hydrogen Energy* **2013**, *38*, 7241–7245. [[CrossRef](#)]
24. Zhao, W.; Wang, X.; Sang, H.; Wang, K. Synthesis of Bi-doped TiO₂ nanotubes and enhanced photocatalytic activity for hydrogen evolution from glycerol solution. *Chin. J. Chem.* **2013**, *31*, 415–420. [[CrossRef](#)]
25. Chen, Q.; Zhou, W.; Du, G.; Peng, L.M. Trititanate nanotubes made via a single alkali treatment. *Adv. Mater.* **2002**, *14*, 1208–1211. [[CrossRef](#)]
26. Kasuga, T.; Hiramatsu, M.; Hoson, A.; Sekino, T.; Niihara, K. Formation of titanium oxide nanotube. *Langmuir* **1998**, *14*, 3160–3163. [[CrossRef](#)]
27. Lee, J.H.; Leu, I.C.; Hsu, M.C.; Chung, Y.W.; Hon, M.H. Fabrication of aligned TiO₂ one-dimensional nanostructured arrays using a one-step templating solution approach. *J. Phys. Chem. B* **2005**, *109*, 13056–13059. [[CrossRef](#)]

28. Macak, J.M.; Tsuchiya, H.; Ghicov, A.; Yasuda, K.; Hahn, R.; Bauer, S.; Schmuki, P. TiO₂ nanotubes: Self-organized electrochemical formation, properties and applications. *Curr. Opin. Solid State Mater. Sci.* **2007**, *11*, 3–18. [[CrossRef](#)]
29. Gong, D.; Grimes, C.A.; Varghese, O.K.; Hu, W.; Singh, R.S.; Chen, Z.; Dickey, E.C. Titanium oxide nanotube arrays prepared by anodic oxidation. *J. Mater. Res.* **2001**, *16*, 3331–3334. [[CrossRef](#)]
30. Zhou, D.; Chen, Z.; Gao, T.; Niu, F.; Qin, L.; Huang, Y. Hydrogen generation from water splitting on TiO₂ nanotube-array-based photocatalysts. *Energy Technol.* **2015**, *3*, 888–895. [[CrossRef](#)]
31. Yang, S.; Ohtani, B. Substitutionally rhodium(IV)-doped titania showing photocatalytic activity toward organics oxidation under visible-light irradiation. *Catal. Today* **2021**, *380*, 25–31. [[CrossRef](#)]
32. Suhag, M.H.; Tateishi, I.; Furukawa, M.; Katsumata, H.; Khatun, A.; Kaneco, S. Photocatalytic hydrogen production from formic acid solution with titanium dioxide with the aid of simultaneous Rh deposition. *ChemEngineering* **2022**, *6*, 43. [[CrossRef](#)]
33. Yamamoto, T.; Katsumata, H.; Suzuki, T.; Kaneco, S. Photoelectrochemical reduction of CO₂ in methanol with TiO₂ photoanode and metal cathode. *ECS Trans.* **2017**, *75*, 31–37. [[CrossRef](#)]
34. Slamet; Tristantini, D.; Valentina; Ibadurrohman, M. Photocatalytic hydrogen production from glycerol-water mixture over Pt-N-TiO₂ nanotube photocatalyst. *Int. J. Energy Res.* **2013**, *37*, 1372–1381. [[CrossRef](#)]
35. Zhao, C.; Luo, H.; Chen, F.; Zhang, P.; Yi, L.; You, K. A novel composite of TiO₂ nanotubes with remarkably high efficiency for hydrogen production in solar-driven water splitting. *Energy Environ. Sci.* **2014**, *7*, 1700–1707. [[CrossRef](#)]
36. Wang, Q.; An, N.; Bai, Y.; Hang, H.; Li, J.; Lu, X.; Liu, Y.; Wang, F.; Li, Z.; Lei, Z. High photocatalytic hydrogen production from methanol aqueous solution using the photocatalysts CuS/TiO₂. *Int. J. Hydrogen Energy* **2013**, *38*, 10739–10745. [[CrossRef](#)]
37. Chen, W.T.; Chan, A.; Sun-Waterhouse, D.; Moriga, T.; Idriss, H.; Waterhouse, G.I.N. Ni/TiO₂: A promising low-cost photocatalytic system for solar H₂ production from ethanol-water mixtures. *J. Catal.* **2015**, *326*, 43–53. [[CrossRef](#)]
38. Wei, P.; Liu, J.; Li, Z. Effect of Pt loading and calcination temperature on the photocatalytic hydrogen production activity of TiO₂ microspheres. *Ceram. Int.* **2013**, *39*, 5387–5391. [[CrossRef](#)]
39. Indira, K.; Mudali, U.K.; Nishimura, T.; Rajendran, N. A review on TiO₂ nanotubes: Influence of anodization parameters, formation mechanism, properties, corrosion behavior, and biomedical applications. *J. Bio-Tribo-Corros.* **2015**, *1*, 28. [[CrossRef](#)]
40. Ribeiro, B.; Offoiach, R.; Rahimi, E.; Salatin, E.; Lekka, M.; Fedrizzi, L. On growth and morphology of TiO₂ nanotubes on Ti₆Al₄V by anodic oxidation in ethylene glycol electrolyte: Influence of microstructure and anodization parameters. *Materials* **2021**, *14*, 2540. [[CrossRef](#)]
41. Shi, H. Formation mechanism of anodic TiO₂ nanotubes. *Adv. Eng. Res.* **2017**, *123*, 785–788.